EasyChair Preprint

№ 4419

CFD Investigation on Optimization of Pipe Pattern in Radiant Cooling System

Prashant R. Nawale, Sudesh B. Powar and Pramod P. Kothmire

October 17, 2020

CFD investigation on optimization of pipe pattern in radiant cooling system

Prashant R Nawale[1], Sudesh B Powar[1], Pramod P Kothmire[1]

[1]School of Mechanical and Civil Engineering, MIT Academy of Engineering, Alandi(D), Pune, India 412105

Abstract. The radiative heat transfer process has so far been proven effective and efficient in the Heating, Ventilation and Air Conditioning industry and therefore it has been used for air conditioning applications. Radiant floor heating systems could be even effective over the conventional air conditioning systems as the water in motion that is used in the radiative systems have more energy carrying capacity compared to air in motion used in conventional air conditioning system. In the present study, the computational fluid dynamics analysis of a radiant cooled room is carried out by varying the design of pipe patterns and their simulations for cooling the typical room has been carried out. Eleven such pipe patterns were analyzed for both steady and unsteady conditions. A three dimensional geometrical model of specified dimension was used for the analysis. Ordinary heat loads from the light bulb, window, floor, human and laptop are defined in the model. Different loads such as energy, buoyancy, and radiation are also included in the simulation and thermal boundary conditions are applied on ceiling and walls. Also, the effect on the analysis when the room is unoccupied and occupied was studied by considering the factors such as air velocity, inlet water temperature as constant. This study validated by the difference between the inlet and outlet of water and air temperature respectively. The temperature distribution pattern in a room due to the mixed flow design pipe pattern was found to be most effective for cooling and better comfort conditions.

Keywords: CFD analysis, pipe patterns, design of pipe pattern, Radiant cooling, Heat loads, Boundary conditions.

1 Introduction

The radiative heat transfer principle is emerging technology used in the Air Conditioning system and has been proven effective. For heating and cooling application, the Hydronic systems i.e. water-based systems are practically in use. In this case, the pipes carrying water may be embedded in the building structures like floor ceilings or walls. Radiant panels are also in use which has metal pipes integrated into it. But the radiative heat transfer process may also have few limitations like a condensation of water may take place around the radiating panels.

An experiment on the building of a software firm INFOSYS Ltd has been successfully carried out in Hyderabad by Guru Prakash Sastry[20]. The building was geometrically symmetrical and hence in the one half of a building conventional air conditioning system was used and in the other half portion Radiative air conditioning system was used so that a direct comparative analysis could be done. It was found that the radiative air conditioning system consumes 33 percents less energy as compared to the conventional air conditioning system also other factors such as Human comfort, cost-effectiveness were also found to be more effective[19]. The computer simulation was done by Angelo Zarella et al.[1] where the dehumidification system was used in integration with the radiative cooling system for three Italian climate zones. The conclusion was made that the partial or latent heat load is transferred to the dehumidifier and the remaining to the radiative cooling system. But in terms of the cost and space, the system may be inconvenient for practical use.

Xiazhou et al.[2] developed a simplified model by using conduction shape factor with which surface temperature and heat transfer of radiant floor heating or cooling systems could be calculated. The graphs were plotted such as the pipe space versus thermal resistance of radiant floor and the thickness of screed versus thermal resistance of the radiant floor. It was observed that the screed thickness has no impact on the thermal resistance whereas the pipe spacing and average water temperature had a great effect on the thermal resistance. Prateek Srivastava et al.[3] analyzed the system where the radiative cooling system was used in integration with evaporative cooling systems for different Indian climate zones. Two main systems first chiller operated Radiative cooling system and second cooling tower operated radiative cooling systems were analyzed for the study. The cooling tower operated system gave 7 percent of annual savings in hot and dry climate followed by 11 percent and 20 percent in composite and temperate climate respectively.

Laia Haurie et al.[4] studied the fire behavior of the different fraction of the Phase change material with mortar for the radiant floor systems. With the increase in the fraction of the PCM the thermal diffusivity reduces still the PCM could be used in radiant floor system with some protection. Jovan Pantelic et al.[5] performed an experiment in which he studied the effect of the direct solar radiation on the cooling capacity. It was observed that when the solar radiations come in direct contact with the floor the cooling capacity increases from 32 W/m^2 to 110 W/m^2. Also, the use of high-speed ceiling fans increased the cooling capacity by 12 percents.

Bladamir Romas Alvadaro et al.[6] did a study of liquid-cooled heat sinks of microchannels used in solar cells or other electronic fuel cells. Eight different flow channels were analyzed using ANSYS software and heat flow and distribution pattern was studied. The best effective pattern was selected as a reference for the pipe patterns used in our analysis. Baisong Ning et al.[7] developed a method for calculating cooling load using the heat balance method. A flow chart was constructed keeping into consideration the ISO standards and then the model was solved using MATLAB. This method helps us in designing and sizing the Radiant cooling systems by calculating the

cooling loads. It was also concluded that when this process is adapted the hydronic cooling load would reduce by 16 percent. Wei-Hwa Chiang et al.[8] studied how the Inlet water temperature and its flow rate would affect the cooling efficiency of a Radiant ceiling system. Five different flow rates and five different inlet water temperatures were taken and analyzed for a vertical temperature gradient. The inlet water with temperature 18 degrees Celsius and with flow rate 100LPM was found to be more efficient.

In this study the main focus is on to cool down the temperature of conditioned space up to or below than 24 degree Celsius so that human feels comfort inside the conditioned space. Study plans different pipe patterns being used below the floor surface so that the temperature decreases at the occupied floor. It is based on the pipe pattern as none of the researcher has not been studied the effect of pipe pattern inside the room by using computational fluid dynamics tool. The previous research says that they had done simulations by considering any of the pattern instead of fifteen (figure 3) patterns used inside the condi- tioned space. This paper focused on the temperature distribution using CFD with single phase fluid, the above review shows that no such analysis for differ- ent patterns was carried out. The present study focused on floor temperature and inside the thermal condition of the air and water. With the help of the CFD simulation tool, we have investigated the optimum floor pattern for tem- perature distribution which should be maintained in a room to get sufficient residence time to cool down the floor temperature. Also, we co-related one of the patterns concerning industrial floor surface temperature. Though, caution has to be taken on the air inlet conditions and water inlet condition.

2 Methodology

A 3D geometric CATIA model having dimensions 4x3x3m(lxbxh) was used for the analysis. All the dimensions are in millimeters as shown in figure 1.
The schematic diagram shows us an un-occupied room. This figure is essential to view the location and dimensions of the door, window, bulb, air and water inlets outlets respectively. Below the floor surface, a 75mm thick is provided to burried polybutylene pipes while construction and the insulation is given in beneath. Air is imposed into the room through a square duct of area 0.16 mm^2 and air is extracted with the same size of duct. Figure 2, shows us the pattern in which the room is occupied by the Table, Human, Chairs, and laptop.

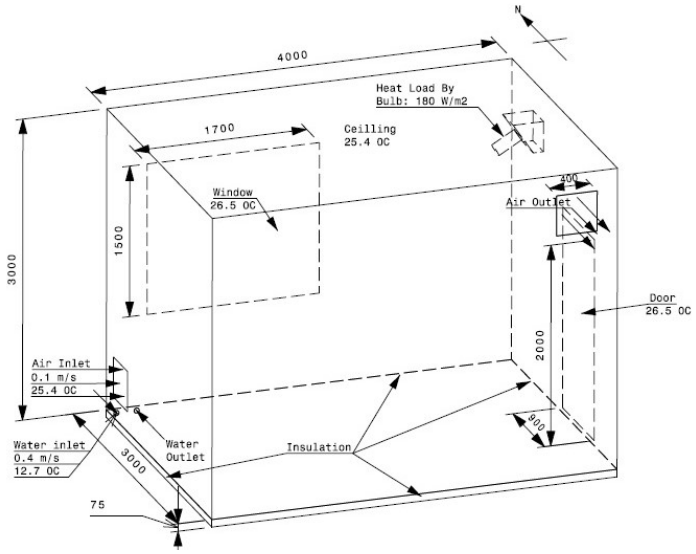

Fig. 1. Schematic Diagram of room when the room is unoccupied

The analysis was done in two types one was of the room with no occupants and the other was with occupants. Eleven such pipe patterns were analyzed for both the above cases using the ANSYS-Fluent software. In meshing the pipe joints have more finely meshed for better results. For flexible results output, the input air and water temperatures and other ambient temperatures were considered almost constant.

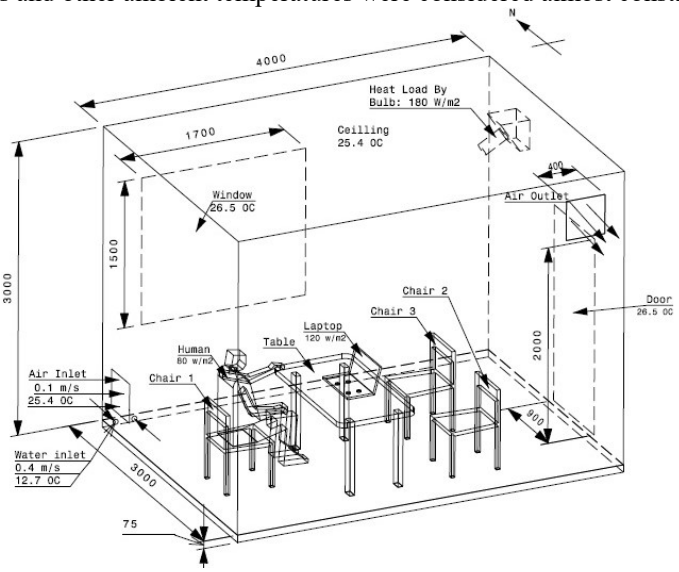

Fig. 2. Schematic Diagram of room when the room is occupied with human, electric component, wooden chairs and table

To get the optimum results, the inlet and outlet positions of water and air are needed to study. Refer to table 6 and table 8 for the temperature of air and water outlets. For both occupied and unoccupied room, different pattern design (figure 3) is used to get temperature distribution.

2.1 Nomenclature for pipe patterns

As per the shape of the pipe pattern we got different names for the eleven cases (figure 3). Case 1 & 8 Serpentine Pipe Pattern Case 2 Counterflow Pipe Pattern Case 3 & 4 Double Serpentine Pipe Pattern Case 5 Mixed flow Pipe Pattern Case 6 & 7 Distributor flow Pipe Pattern Case 9 & 10 Double-wall Ser- pentine Pipe Pattern Case 11 Triple wall Serpentine Pipe Pattern.

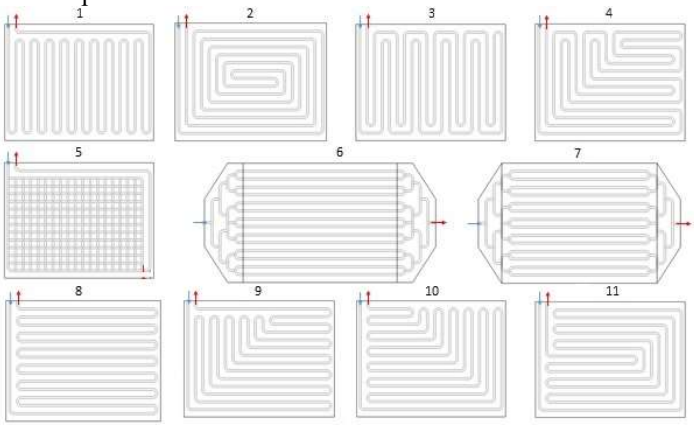

Fig. 3. Different designs of pipe pattern for cooling water circulation through radiant pipe

The distance between the two pipes in each pipe pattern is 200mm in all the above cases and also the clearance from side walls are the same.

2.2 Meshing of Geometry

The mesh contains polyhedral meshing elements for simulations. For 3D (figure 1) modeling here we used CATIA V5. From figure 4 we can observe that water enters at the inlet this water split through holes of the distributor.

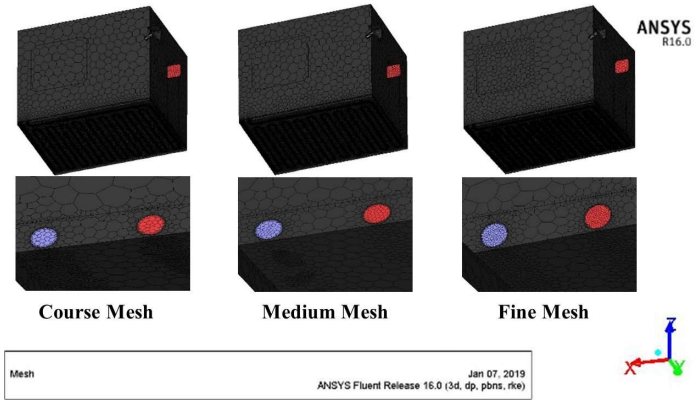

Fig. 4. Polyhedral meshing of geometry

The fine mesh was generated on a model with near about 4754286 nodes and 878123 elements. It is performed by ANSYS workbench to get the course, medium, and fine meshing as shown in figure 4. Fluent is used as a solver. Tetrahedron mesh is used for this geometry. For occupied and unoccupied room also have a similar meshing process.

3 CFD Model

Following CFD models were analyzed using the Energy equation, viscous model and radiation model. When energy equations are activated then the temperature variations in the finite volume method are viewed. For the viscous model, two equations of the K-Epsilon model including near-wall treatment with standard wall functions for turbulence were selected.

Table 1. Material used and their properties[9].

Materials	Density (kg/m^3)	Specific Heat (J/kgK)	Thermal Conductivity (W/mK)
Air	1.225	1006.43	0.0242
Concrete	2400	800	0.6
Glass	2531	840	0.8
Human	985	3600	1.06
Insulation	48	790	0.01
Polybutylene	940	1421	0.2741
Water	998.2	4182	0.6
Wood	700	2310	0.173

Table 2. Inlet boundary conditions of fluid zones.

Zone Boundary	Inlet Velocity (m/s)	Inlet Temperature (Degree Celsius)	Thermal Emissivity

Air	0.1	25.4	0.9
Water	0.4	12.7	0.98

Table 3. Heat fluxes given to boundary surfaces.

Heating Surfaces	Boundary Material	Heat Flux (Degree Celsius)	Thermal Emissivity
Bulb	Glass	180	0.9
Human	Skin properties	40	0.97
Laptop	Glass	120	0.9

The residual plot for every simulation approaches to zero as several iterations increases, therefore, the flow converges. Every simulation was carried out until the steady-state was achieved. In the residual plot after convergence, the graph of energy equations decreases below the 0.0001.

Table 4. Temperatures in degree Celsius given to boundary surfaces.

Boundary	Material	Temparature (Degree Celsius)	Emissivity
Chairs (Three)	Wood	23	0.78
Ceiling	Concrete	25.4	0.92
Door	Wood	26.5	0.8
Insulation	Insulation	23	0.88
Table	Wood	23	0.78
Wall	Concrete	24.2	0.9
Window	Glass	26.5	0.85

3.1 Analysis of 3D-Model

The analysis of the model was done by flow and turbulence equations. Flow converges at the same mass flow rate at inlet and outlet with the help of the continuity equation. Air inlet and outlet temperature conditions have also been considered. Temperature Distribution on the human body is shown in contours. Water temperature contours were applied for temperature distribution. The residual plot was done for the momentum equation, energy equation, and flow equation.

Table 5. Average temperature of plane at different height from the floor surface.

Z from Floor surface	T_{avg} (Degree Celsius)
30	296.95733
60	297.04656
90	297.11219
120	297.17441
150	297.22805

180	297.26264

Planes were located at different heights z-axis for temperature gradient planes. Planes are at 0.3, 0.6, 0.9, 1.2, 1.5, 1.7 m from floor surface.

3.2 Governing equations and boundary conditions

The energy conservation equation for solid regions[4], accounting for volumetric heat release can be written as:

$$K_s\left(\frac{\partial^2 T}{\partial x^2}+\ \frac{\partial^2 T}{\partial y^2}+\ \frac{\partial^2 T}{\partial z^2}\right)=0 \quad \ldots(1)$$

The energy conservation equation for a fluid domain[3], accounting for volumetric heat release, can be written as:

$$u\frac{\partial(\rho_f C_f T_f)}{\partial x}+v\frac{\partial(\rho_f C_f T_f)}{\partial x}+w\frac{\partial(\rho_f C_f T_f)}{\partial x}=k_f\frac{\partial^2 T_f}{\partial x^2}+k_f\frac{\partial^2 T_f}{\partial y^2}+k_f\frac{\partial^2 T_f}{\partial z^2} \ldots(2)$$

The fluid continuity equation[6], accounting for flow, can be written as:

$$\frac{\partial(\rho_f u)}{\partial x}+\frac{\partial(\rho_f v)}{\partial y}+\frac{\partial(\rho_f w)}{\partial z}=0 \quad \ldots(3)$$

$$\frac{\partial(\rho_f u_i)}{\partial x_i}=0 \quad \ldots(4)$$

The momentum equations[2] in x, y and z direction, accounting for momentum, can be written as:

$$u\frac{\partial(\rho_f u)}{\partial x}+v\frac{\partial(\rho_f u)}{\partial y}+w\frac{\partial(\rho_f u)}{\partial z}=\frac{\partial\left(\mu_f\frac{du}{dx}\right)}{\partial x}+\frac{\partial\left(\mu_f\frac{du}{dy}\right)}{\partial y}+\frac{\partial\left(\mu_f\frac{du}{dz}\right)}{\partial z}-\frac{\partial p}{\partial x}(5)$$

$$u\frac{\partial(\rho_f v)}{\partial x}+v\frac{\partial(\rho_f v)}{\partial y}+w\frac{\partial(\rho_f v)}{\partial z}=\frac{\partial\left(\mu_f\frac{dv}{dx}\right)}{\partial x}+\frac{\partial\left(\mu_f\frac{dv}{dy}\right)}{\partial y}+\frac{\partial\left(\mu_f\frac{dv}{dz}\right)}{\partial z}-\frac{\partial p}{\partial y} \ldots(6)$$

$$u\frac{\partial(\rho_f w)}{\partial x}+v\frac{\partial(\rho_f w)}{\partial y}+w\frac{\partial(\rho_f w)}{\partial z}=\frac{\partial\left(\mu_f\frac{dw}{dx}\right)}{\partial x}+\frac{\partial\left(\mu_f\frac{dw}{dy}\right)}{\partial y}+\frac{\partial\left(\mu_f\frac{dw}{dz}\right)}{\partial z}-\frac{\partial p}{\partial z}(7)$$

$$\frac{\partial(\rho_f u_i u_j)}{\partial x_j}=\frac{\partial}{\partial x_j}(-\rho\overline{u'_i u'_j})+\frac{\partial}{\partial x_j}\left[\ \mu\left(\frac{\partial u_i}{\partial x_j}+\frac{\partial u_j}{\partial x_i}-\frac{2}{3}\delta_{ij}\frac{\partial \mu_k}{\partial x_k}\right)\right]-\frac{\partial p}{\partial x_i}\quad \ldots(8)$$

There are three zones air, concrete, and water out of which concrete has a solid zone and the rest of the zones are fluid zones. For these fluid zones, we have considered the outlet as a pressure outlet and inlet as a velocity inlet. As per the referred research paper[3] the velocity between 0.3 to 0.4 meter per second gives the better temperature distribution by water to the floor surface. The floor surface and water pipe surface are coupled to the solid zone and fluid zones. Kinematic Viscosity of air and water are $1.7894e^{-05}$ and 0.001003 Kg/ms respectively.

3.3 Material Properties

From table 1, these are the properties of the materials consisting of the room. After a few research survey, the most appropriate insulation was selected based on its density specific heat and thermal conductivity. The unit of properties is in S.I system. Thermal emissivity for floor surface is 0.9 and the material used is concrete. The water pipe used in the model is considered as polybutylene material and its thermal emissivity is 0.96.

3.4 Boundary Conditions

The table 2 below shows us the boundaries i.e. the contents of the room. For the boundary conditions of the heat loads (Human, Bulb, and Laptop), heat flux and thermal emissivity were considered.
For the other objects which aren't supposed to impose a considerable heat load, for them, the average surface temperature and the thermal emissivity are described. The normal Surface area of a human being is 1.8 m^2, in given model the surface area is 2 m^2 hence the heat flux on the human surface is up to 80 Watt.

4 Grid independency test

In grid independency test the mass flow rate of air and water inlet due to area varies as the number of cells increases. A smooth temperature contour plot is achieved as the cells increases but due to system specifications, we cannot increase the cells beyond the specified limit. The mass-weighted average static temperatures within

the air zone and water zone versus the number of cells were plotted.

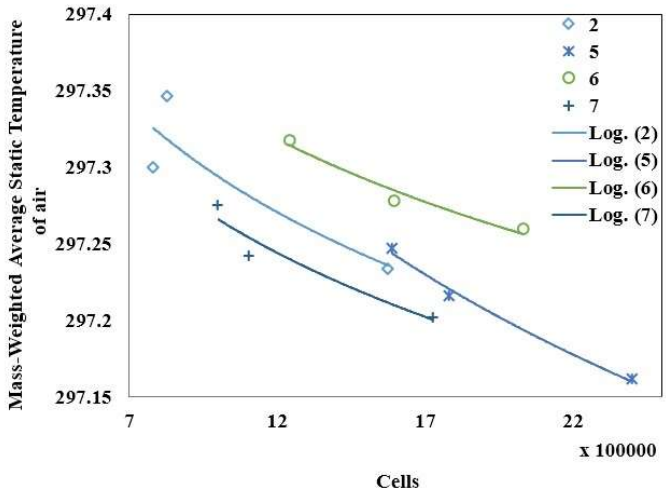

(a) Mass Weighted Average Static Temperature of water with cells count of the pattern

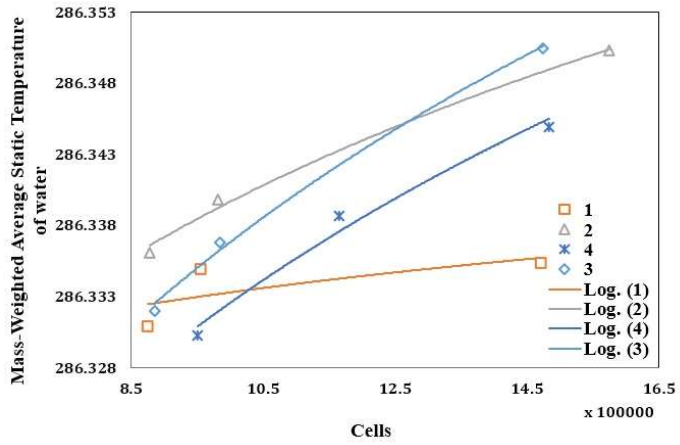

(b) Mass Weighted Average Static Temperature of air with cells count of the pattern

Fig. 5. Mass Weighted Average Static Temperature with cells count of pattern

The mass-weighted average static temperature inside the water zone increases as the number of cells increases whereas the mass-weighted average static temperature inside the air zone decreases as the number of cells increases. The cross-section of inlet and outlet of water and air changes as grid size increases hence the mass flow rate changes. The cross-section of inlet and outlet of water pipe tends to become circular but the grid size can not increase much due to computational restrictions.

5 CFD Analysis

Figure 6, indicates the temperature distribution inside the pipes for different patterns. With the help of the color-map situated on the left side of the figure, the temperature distribution can be well understood respective of the colors. Twenty levels are used in the color map. The low-temperature field can be determined by the Blue color indication similarly for the high-temperature fields red color serves as an indication. From figure 6, it is seen that as the temperature of the water increases from inlet to outlet due to the heat absorbed, the color tends to change from Blue to Red.

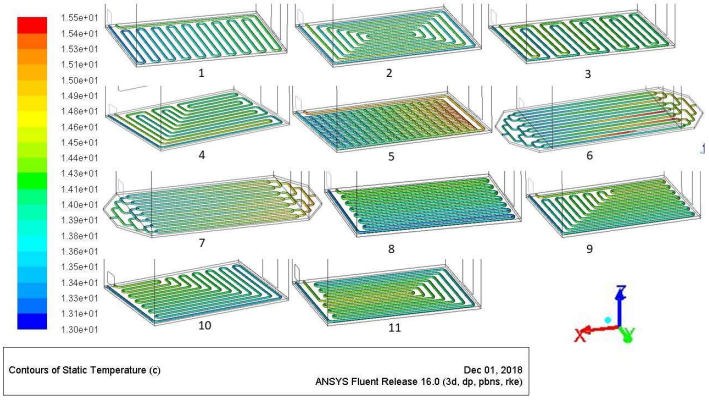

Fig. 6. Contours of temperature distribution through pipe

As seen in figure 7, the color pattern here helps us to understand the heat pattern inside the room for different cases. It can be seen that the floor temper- ature is cooler than the walls also a quite redness near the door and the window indicates the temperature is comparatively high. The temperature distribution on the surface of human is shown above. The second, fifth and ninth case was found to be comfortable when the human is occupied.

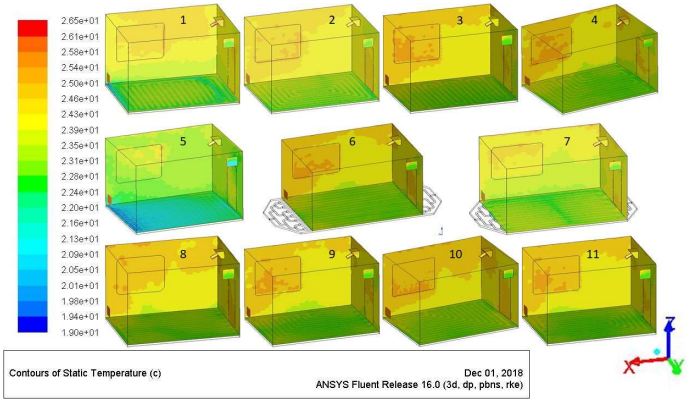

Fig. 7. Contours of temperature distribution at the floor and walls of the room

As it is visible in figure 8, the region near the legs of the human is blue as they are

situated close to the floor. This indicates that the heat removal takes place from bottom to top of the human body.

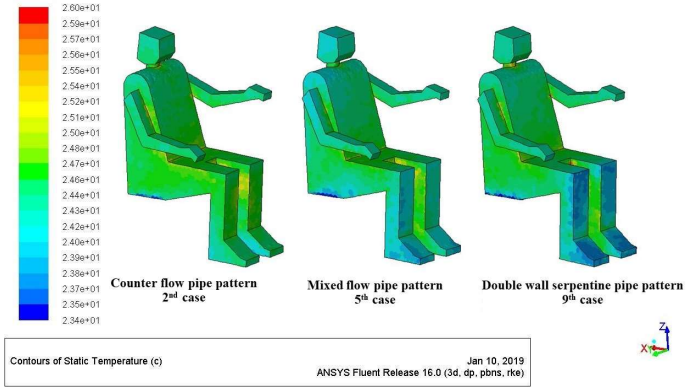

Fig. 8. Contours of temperature distribution on Human Body

Area-Weighted Average Static Temperature at floor surface is almost 294.33 degrees Celsius this increases from floor to ceiling as shown in table 5. Figure 9, is a plot between temperature and length for eight patterns. The length of the pipes in all the eight cases is almost the same. This graph helps us to understand the behavior of the heat been absorbed along the length of the pipe. From figure 9, it is observed that the absolute temperature at the axis is increased across the length of the pipe. The small spikes in the graph indicate the temperature at a turn in the pipe. At this turn-point due to the turbulence more amount of heat is removed. From this, it is concluded that if we increase the number of turns more heat could be removed.

6 Results and Discussions

For the steady-state, after the convergence, the mass flow rate at inlet and outlet of air and water was achieved almost the same due to the same surface area of air and water, inlets and outlets. The mass flow rate of air is 0.01951 kg/s and the mass flow rate of water is 0.803 kg/s.

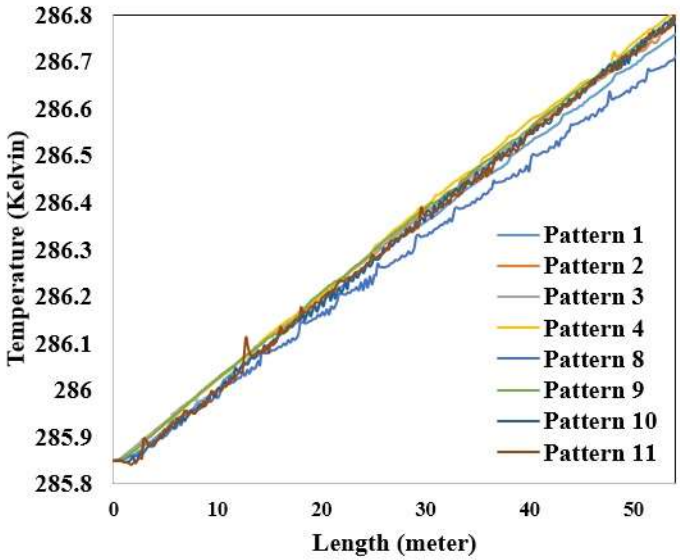

Fig. 9. Temperature at center of pipe with length of pipe

An increasing slope in the graph of figure 10 between 0 to 100 seconds indicates that the temperature increases for the first 100 seconds due to heating surfaces inside the room and later on the temperature tends to decreases slowly as there is no heat generation. As compared to the other patterns it is seen from the graph that the average temperature of the air is lower than means of this pattern has been more effective in case of the heat removal with the help of water circulation.

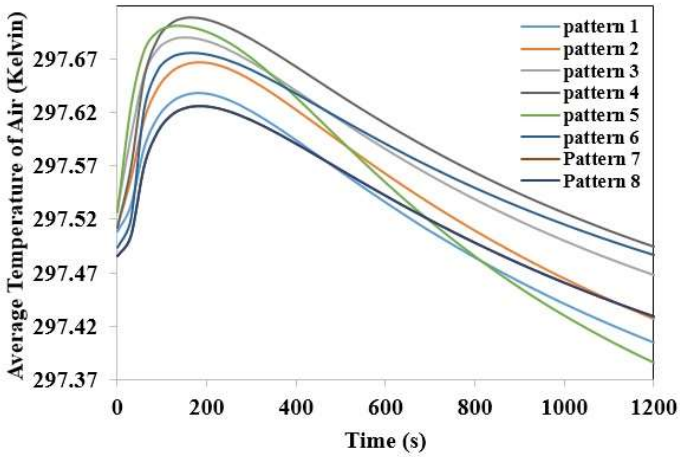

Fig. 10. Area weighted average temperature of air with time of pattern

The graph of figure 11, not only shows us the heat being removed with time but also serves as an analysis of the model. The unsteady state was analyzed for eight patterns

following results were obtained. As concluded from the figure 10, the avg temp of water is more during the first 100s similar results were obtained for the air as well. A steep rise is seen in the graph at the start and later on again the slope. This means the avg temp of air is initially high and decreases as time increases. In this plot too, it is seen that the plot-line for the fifth case lies at the bottom-most position indicating that the average temperature is the lowest compared to the other cases.

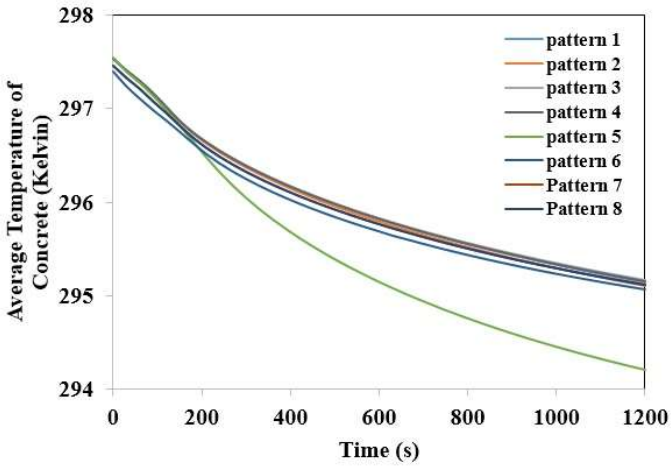

Fig. 11. Area weighted average temperature of concrete with time of pattern

As the pipes are situated between the concrete the plot between the average temperatures of concrete vs time helps us to validate the above-obtained results. It would be contradictory to the previously plotted results if in this (figure 10) plot the fifth case was not found efficient. Fortunately, figure 12 also shows the same results that the average temperature of the floor in the fifth pattern is the least pattern.

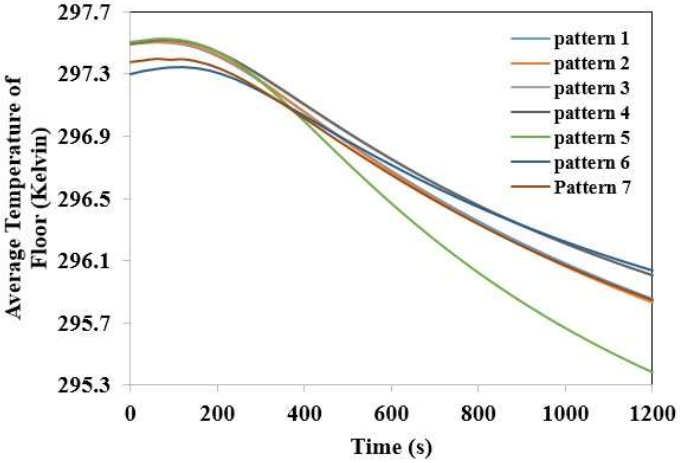

Fig. 12. Area weighted average temperature of floor with time of pattern

The average temperature of the concrete tends to decrease with the time- lapse. The average temperature seems to be reduced until a lapse of 1200 seconds (twenty minutes) whereas in the case of the air and water it reduces up to the first hundred seconds. Even for the concrete, the least average temperature was to be noted for the fifth case. The graph shown in figure 12 is the plot between the average temperatures of floor vs time. It is a natural behavior that the average temp of the floor reduces as time elapses. This graph is plotted up to 1200 seconds was taken.

The mass flow rate and velocity of water and air are almost considered to be constant for all the cases. The heat removal takes place mainly due to water. The negative sign in the table indicates that the heat is being added by the air. The maximum amount of heat removal takes place in the fifth case. The readings for the unsteady state was taken for two-time intervals of five and ten minutes. The unsteady state was analyzed for five patterns following results were obtained.

Table 6. Heat Removal calculations in watt for all patterns when the room is unoccupied.

Case		1	2	3	4	5	6	7	8	9	10	11
Mass flow rate	Air inlet						0.02					
(kg/s)	Water inlet						0.8					
Velocity	Air inlet						0.1					
(m/s)	Water inlet						0.4					
	(a) Air_{in}						298.5					
Temperature	(b) W_{in}						285.85					
(Kelvin)	(c) Air_{out}	285.85	296.61	296.52	296.48	296.54	296.57	296.56	296.57	296.56	296.59	296.50
	(d) W_{out}	288.26	288.18	288.18	288.23	288.42	288.19	288.24	288.09	288.21	288.06	288.21
Temperature-	(c)-(a)	-1.99	-1.94	-2.03	-2.08	-2.01	-1.99	-1.99	-1.99	-1.99	-1.97	-2.05
difference	(d)-(b)	2.41	2.33	2.33	2.38	2.57	2.34	2.39	2.24	2.36	2.21	2.36
Heat removed by air (w)		-40.02	-39.07	-40.79	-41.76	-40.45	-39.95	-40.11	-39.88	-40.14	-39.55	-41.21
Heat removed by water (w)		8088.3	7827.6	7828.6	7987.4	8631.4	7848.4	8023.5	7520.7	7923.1	7428.9	7914.3

From the table 6, we observe that again the maximum amount of heat is being removed from the fifth case. Till the first interval maximum heat is removed and as the time increases the heat removal rate decreases because later on the heat is not generated by any source into the conditioned space.

Following table 7 shows the results for the steady-state when the human and other electronic component is inside the room. From the above table, it is observed that the maximum amount of heat is being removed in the fifth case. As air already has a temperature of 25.4 Degree Celsius not much appreciable amount of heat is added to the room.

Table 7. Heat Removal calculations in watt for all patterns when the room is occupied.

Case		1	2	3	4	5	6	7	8	9	10	11
Mass flow rate	Air inlet						0.02					
(kg/s)	Water inlet						0.8					
Velocity	Air inlet						0.1					
(m/s)	Water inlet						0.4					
Temperature	(a) Air_{in}						298.5					

(Kelvin)	(b) W_{in}					285.85						
	(c) Air_{out}	285.85	296.61	296.52	296.48	296.54	296.57	296.56	296.57	296.56	296.59	296.50
	(d) W_{out}	288.26	288.18	288.18	288.23	288.42	288.19	288.24	288.09	288.21	288.06	288.21
Temperature-	(c)-(a)	-1.91	-1.99	-1.98	-1.91	-1.98	-2.01	-2.01	-2	-2.4	-1.97	-2.12
difference	(d)-(b)	2.30	2.34	2.37	2.29	2.47	2.41	2.41	2.36	2.37	2.34	2.32
Heat removed by air (w)		-38.34	-39.95	-39.78	-38.53	-39.78	-40.45	-40.45	-40.33	-48.31	-39.57	-42.76
Heat removed by water (w)		7713.6	7848.4	7944.4	7689.8	8287.6	8085.2	8085.2	7910.6	7956.1	7865.6	7803.4

The heat removal for the eighth case is from South to North direction. For the second case, the heat is being extracted from outwards towards the center. The third and fourth case comes under double serpentine pattern; in the third case the heat is being removed similar to the first case but here there is more equal temperature distribution observed. In the fourth case due to the arrange- ment of pipe, the cold and hot water pipe comes in contact and a better heat transfer is achieved between them so the temperature here is equally distributed but not centralized as in counter flow pattern. In the distributor pattern for the sixth case, the water is distributed such that the water flows parallel below the floor, but due to less surface area of the pipe below the floor, the heat removed is less. When the seventh case is studied it was found that it is better as compared to the sixth one because more turbulence takes place at the end corners of the pipes and also due to 20 percent more surface area.

7 Conclusions

After the analysis of eleven cases with and without occupants of pipe patterns it was found that the fifth case i.e., mixed flow pattern was more efficient than other patterns. It removes 8 percent more heat than other cases, because the surface area of this pattern is 30 percents more than other patterns. If the almost same surface area is considered for the other eight cases the second counter flow pattern is more efficient for temperature distribution inside the conditioned space because the temperature is equally distributed on the floor. Serpentine pattern included two cases first and the eighth case, in the first case the heat is being removed from the west side to the east side that's why the temperature on the west side is less as compared to the east side. Double-wall serpentine consists of two cases ninth and tenth, wherein the ninth case the temperature is distributed from South-west corner to North-east corner and for the tenth case the heat is removed from south-east corner to north-west corner. Triple wall serpentine i.e., the eleventh simulated case the heat is being removed from all three directions and accumulated towards the west wall. But still one factor i.e., the position of the occupant is important to decide the type of flow pattern despite this fifth pattern was found more effective. Also, when the analysis was done for the occupied room the ninth case was found most effective amongst all because the occupant is located towards the southwest corner where maximum heat is removed.

References

1. Angelo Zarrella, Michele De Carli, Clara Peretti, Radiant floor cooling coupled with dehumidification systems in residential buildings: A simulation-based analysis, Energy Conversion and Management 85 (2014) 254 – 263.
2. Xiaozhou Wu, Jianing Zhao, Bjarne W. Olesen, Lei Fang, Fenghao Wang, A new simplified model to calculate surface temperature and heat transfer of radiant floor heating and cooling systems, Energy and Buildings 105 (2015) 285 - 293.
3. Prateek Srivastava, Yasin Khan, Mahabir Bhandari, Jyotirmay Mathur, Ranaveer Pratap, Calibrated simulation analysis for inte- gration of evaporative cooling and radiant cooling system for differ- ent Indian climatic zones, Journal of Building Engineering 19 (2018) 561 – 572.
4. Laia Haurie, JavierMazo, M´onicaDelgado, Bel´enZalba, Fire behav- ior of a mortar with different mass fractions of phase change material for use in radiant floor systems, Energy and Buildings 84 (2014) 86– 93.
5. Jovan Pantelic, Stefano Schiavon, Baisong Ning, Eleftherios Bur- dakis, Paul Raftery, Fred Bauman, Full scale laboratory experiment on the cooling capacity of a radiant floor system, Energy Buildings 170 (2018) 134 – 144.
6. Bladimir Ramos-Alvarado, Peiwen Li, Hong Liu, Abel Hernandez- Guerrero, CFD study of liquid-cooled heat sinks with micro channel flow field configurations for electronics, fuel cells, and concentrated solar cells, Applied Thermal Engineering 31 (2011) 2494 - 2507.
7. Baisong Ning, Youming Chen, Cooling load calculation for inte- grated operation of radiant and fresh air systems, Procedia Engi- neering 205 (2017) 2987 – 2994.
8. Wei-Hwa Chiang, Chia-Ying Wang, Jian-Sheng Huang, Evaluation of cooling ceiling and mechanical ventilation systems on thermal comfort using CFD study in an office for subtropical region, Building and Environment 48 (2012) 113 - 127.
9. Maxime Tye-Gingras, Louis Gosselin, Comfort and energy consump- tion of hydronic heating radiant ceilings and walls based on CFD analysis, Building and Environment 54 (2012) 1 - 13.
10. Dengjia Wang, Chunjin Wu, Yanfeng Liu, Penghao Chen, Jiaping Liu, Experimental study on the thermal performance of an enhanced convection overhead radiant floor heating system, Energy and Build- ings 135 (2017) 233 – 243.
11. Tomohiro Kobayashi, Kazuki Sugita, Noriko Umemiya, Takashi Kishimoto, Mats Sandberg, Numerical investigation and accuracy verification of indoor environment for an impinging jet ventilated room using computational fluid dynamics, Building and Environ- ment 115 (2017) 251 - 268.
12. Ahmed Qasim Ahmed, Shian Gao, Numerical investigation of height impact of local exhaust combined with an office work station on energy saving and indoor environment, Building and Environment 122 (2017) 194 – 205
13. Mehdi Pazhoohesh, Cheng Zhang, A satisfaction-range approach for achieving thermal comfort level in a shared office, Building and En- vironment 142 (2018) 312 - 326.
14. Jianhua Fan, Christian Anker Hviid, Honglu Yang, Performance analysis of a new design of office diffuse ceiling ventilation system, Energy and Buildings 59 (2013) 73– 81.
15. Ali F. Alajmi, Faisal A. Baddar, Raed I Bourisli, Thermal comfort assessment of an office building served by under-floor air distribution (UFAD) system - A case study, Building and Environment 85 (2015) 153 - 159.
16. Ooi Yongson, Irfan Anjum Badruddin, Z.A. Zainal, P.A. Aswatha Narayana, Airflow analysis in an air conditioning room, Building and Environment 42 (2007) 1531 – 1537.
17. Xingwang Zhao, Wei Liu, Dayi Lai, Qingyan Chen, Optimal design of an indoor environment by the CFD-based adjoint method with area-constrained topology and cluster analysis, Building and Envi- ronment 138 (2018) 171 – 180.
18. John Calautit, Angelo Aquino, Dominic O'Connor, Sheen Ca- baneros, Sally Shahzad, Saeed Wazed, Tom Garwood, Katrina Calautit,Ben Hughes, Indoor environmental quality (IEQ) analy- sis of a low energy wind catcher with horizontally-arranged heat transfer

devices, Energy Procedia 142 (2017) 2095 – 2101.
19. Lounes Koufi Zohir Younsi, Yassine Cherif, Hassane Naji, Numerical investigation and analysis of indoor air quality in a room based on impinging jet ventilation, Energy Procedia 139 (2017) 710 – 717.
20. Guruprakash Sastry, First radiant cooled commercial building in india – critical analysis of energy, comfort and cost, Environmental and Social Management, (2012).